Optics Communications 435 (2019) 433–440

Contents lists available at ScienceDirect

Optics Communications

journal homepage: www.elsevier.com/locate/optcom

Experiments and simulations of QCW Yb:YAG laser with consideration of transient temperature

Yanchao Wang [a,b], Pengyuan Wang [a], Ying Chen [a], Baichao Zhang [a,b], Dong Liu [a], Zhi Xu [a], Zhonghui Li [a], Xianglong Cai [a], Youbao Sang [a,b], Jingwei Guo [a,*], Ying Huai [a], Wanfa Liu [a]

[a] Key Laboratory of Chemical Lasers, Dalian Institute of Chemical Physics, Chinese Academy of Sciences, China
[b] University of Chinese Academy of Sciences, Beijing 100049, China

ARTICLE INFO

Keywords:
Thermal effects
Transient temperature
Rate equations
Yb:YAG lasers

ABSTRACT

The effects of transient temperature variation of gain medium on quasi-three-level microchip laser were investigated. Firstly, the dynamic behavior with temperature variation and the characteristic of the output power were reported. The numerical simulation results revealed not only the dynamics characteristic of lasing levels, but also the relationship between pump pulse width and output power in equivalent duty cycle. The increments of output power deviated significantly from linear increasing with the pump pulse width. The characteristic of the output power with different duty cycle was compared. Because the heat load was rising with the increase of the duty cycle and high heat load reduced population inversion density, the optical-to-optical efficiency of 9.7% at 50% duty cycle was lower than optical-to-optical efficiency of 15.6% at 7% duty cycle. The calculated and experimental pump power thresholds for output of 1030 nm were discussed. Particularly, the output power calculated by the model with the addition of temperature terms was significantly lower than that simulated by the model without temperature terms. Experimental results have shown a good agreement with the theoretical predictions.

1. Introduction

Ytterbium doped laser medium characterized by no up-conversion and no excited-state absorption plays an important role in high-energy laser regime. The material Yb:YAG works at the quasi-three-level laser system in room temperature [1]. The lower level for lasering of 1030 nm is 612 cm^{-1} above the ground state. About 4.9% particles are populated on the lower level ($^2F_{7/2}$) of lasing at 293 K, and there is serious re-absorption, therefore the temperature is a crucial characteristic for Yb:YAG laser.

In comparison with Nd:YAG, Yb:YAG has smaller absorption cross section and stimulated emission cross section in the same doping concentration. However, Yb^{3+} ions could achieve high doping concentration in YAG base material to overcome this shortage. The quasi-three-level laser system of Yb:YAG for high doping concentration requires higher pumping intensity to overcome threshold and achieve higher efficiency at room temperature than low doping concentration. The threshold of absorbed pump power density is as high as 1.7 kW/cm^3 [2] for a 1 at.% Yb:YAG crystal and 5 kW/cm^3 for a 10 at.% Yb:YAG crystal [1]. In order to achieve high output power, the Yb:YAG laser material should absorb even higher pump power. The heat manage plays a critical role in this case. In contrast to the pump mode of continuous wave (CW), thermal deposition in laser media could be removed effectively in quasi-CW (QCW) mode. The pump pulse width for Nd:YAG is generally ~200 μs, which is approximately corresponding to the lifetime of the upper laser level. Similarly, the optimum pump width for Yb:YAG should also relate with the lifetime of the upper laser level, which is around 0.95 ms [3]. Nevertheless, the pulse width of the high-power pump source of QCW Yb:YAG laser is usually no more than 500 μs, due to difficult thermal management of diode laser pump sources. Thus, it is very important to investigate Yb:YAG laser pumping by different pulse width.

Different from CW mode, the transient temperature of laser materials should vary with time in QCW mode. Because of the re-absorption of the lower lasing level, the variation of transient temperature of laser materials has an important influence on the output power of laser. The power scaling of such a laser is mainly limited by the thermal load and heat removal ability of the gain medium. Laser behavior of different thermal loads were compared by L. Esposito et al. [4]. The laser outputs were further characterized under QCW pumping mode with duty cycle 40%, and CW pumping mode respectively. For increasing duty cycle, all samples showed a declining peak power and slope efficiency. Therefore, it is necessary to investigate of thermal problem, especially under the condition of QCW mode of different pulse width in common duty cycle.

Many numerical calculations and experiments were reported to analyze thermal problems. T.Y. Fan predicted the heat fraction under

* Correspondence to: Key Laboratory of Chemical Lasers, Dalian Institute of Chemical Physics, #457 Zhongshan Road, Dalian, Liaoning Province, 116023, China.
E-mail address: jingweiguo@dicp.ac.cn (J. Guo).

https://doi.org/10.1016/j.optcom.2018.11.012
Received 12 July 2018; Received in revised form 15 October 2018; Accepted 5 November 2018
Available online 20 November 2018
0030-4018/

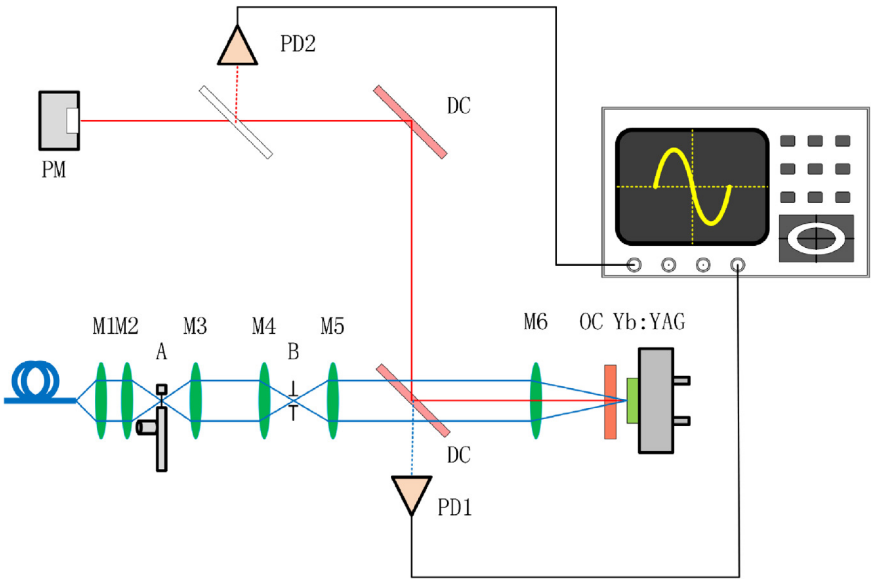

Fig. 1. Schematic diagram of diode-laser pumped Yb:YAG microchip lasers.

lasing and nonlasing process in Nd:YAG and Yb:YAG [5]. M. Innocenzi presented steady-state thermal profiles in both a full numerical solution and an analytic approximation with an assumption of only radial heat flow [6]. A.K. Cousins summarized the effects of pump heat deposition on optical aberrations and thermal stress fracture in end-pumped solid-state laser rods. They chose a non-dimensional form to make results independent of any particular rod materials [7]. M. Schmid developed two different methods using both Taylor series and the integration of differential heating distributions to calculate the temperature distribution and thermal effects [8]. Considerable experiments were carried out to examine laser repetitive pulse heating by S.Z. Shuja. They showed that both the rising rate of surface temperature and temperature increment increased with the duty cycle in the mode of consecutive pulse irradiation [9]. J.L. Li introduced population inversion in the form of the sawtooth time function to investigate the transient temperature profile in CW and end-pump passively Q-switched (PQS) microchip laser. They exposed dynamics of thermal buildup, dependence of the quasi-steady-state temperature rise, the repetitively oscillatory amplitude on the incident pump power and the pulse repetition rate of PQS laser [10]. S.Z. Shuja [9,11] took a numerical method into solving governing equations of heat transfer. It was found that the rising rate of surface temperature was higher and temperature difference was larger for higher duty cycle during the consecutive pulse irradiation. Temperature and stress fields in the irradiated region were predicted for various laser pulse intensity distributions at the workpiece surface. G.Z. Zhu used an analytical model to describe the dynamic behavior of an end-pumped Yb:YAG thin disk laser. The dependence of the fractional thermal load on the temperature of the thin disk crystal and intra-cavity laser intensity was taken into account in their calculation [12]. X.J. Cheng investigated heat conduction, temperature distribution, thermal stress, and thermally induced refractive index of a diode-pumped active-mirror grad-doped Yb:YAG ceramic laser compared to a uniform-doped Yb:YAG ceramic laser. They evidenced a smaller temperature gradient than a uniform-doped Yb:YAG ceramic with the same absorption pump power, which resulted in an higher output energy in the grad-doped Yb:YAG ceramic laser [13]. P. Ferrara developed a procedure allowing 3D numerical analysis of the slab optical properties as a consequence of the thermal load induced by the pump process [14].

In this paper, the transient temperature distribution was numerical simulated. The thermal source density varying with the non-uniform absorption of pump light based on Lambert–beer's law was taken into account. We have built a model based on rate equation, and the re-absorption of the lower lasing levels and transient temperature variation of gain medium were considered in the model. This model allows us to predict the dynamic behavior with temperature varying and the characteristic of the output power under different pump pulse widths and pump currents. The impact of the different pump pulse width on the laser performance was explored using this model. The characteristics of two pump duty cycles were compared and the laser performance with different pulse widths was investigated at duty cycle of 7% in experiment. Experimental results have shown a good agreement with the theoretical predictions.

2. Experiment setup

The schematic setup of the device was outlined in Fig. 1. The laser was an end-pumped system with a plane-parallel cavity. A YAG crystal plate doped with 5% Yb^{3+} was used as the gain media, which has the diameter of 1 cm and the thickness of 0.8 mm. One surface of Yb:YAG crystal was coated for antireflection at both 940 nm and 1030 nm. The other surface was coated for high reflection at both 940 nm and 1030 nm and it was welded to a copper heat sink. A plane mirror with output coupling rate of 5% was used as a cavity mirror. The cavity length was around 3.5 mm. The gain material was longitudinally pumped by a fiber coupled diode laser, which had a core diameter of 400 μm, a numerical aperture of 0.22, and the maximum power in CW mode of 200 W at 940 nm. In Fig. 1, spots A and B were foci of focused pump beam. A chopper wheel was placed at the spot A. Variable pump pulse widths with the different duty cycle can be produced by the chopper wheel. A pin hole was placed at spot B for spatial filtering. The lens M1 ~ M6 was used to focus the pump beam on Yb: YAG crystal. A micron viewer 7290A (Electro physics) was used to measure the profile of pump beam at the position of crystal. The intensity distribution of pump light and fitted result along y direction of the crystal and the laser beam were shown in Fig. 2. The size of pump light on the crystal was proximately 400 μm in diameter. The laser beam focused with the lens of focus length 300 mm was measured by camera SP300 nearby the foci. Waveforms at the wavelength of 940 nm and 1030 nm were detected with photodiode 1 (PD1) and photodiode 2 (PD2), respectively. The wave forms of pump and laser pulse with duty factor 7% and the width of pump pulse 398 μs was shown as Fig. 3. Laser was terminated before the end time of pump pulse. This phenomenon was caused by the thermal sink in the crystal. The laser spectrum of diode laser was measured by a Horiba iHR-320 spectrophotometer, as shown in Fig. 4.

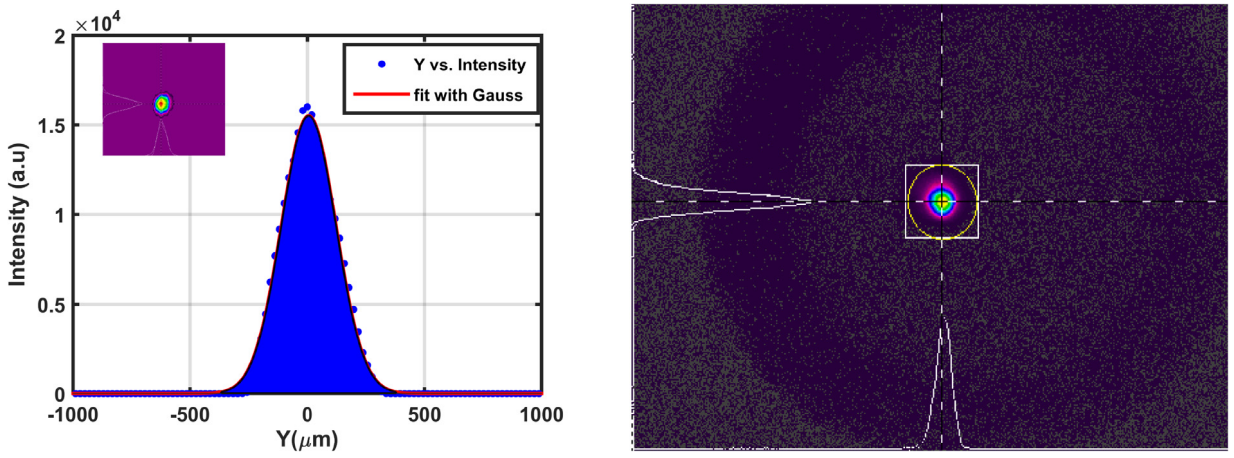

Fig. 2. The intensity distribution of pump light and fitted result along y direction on the crystal, inset: the measured pump beam profile (left); laser beam focused with the lens of focus length 300 mm (right).

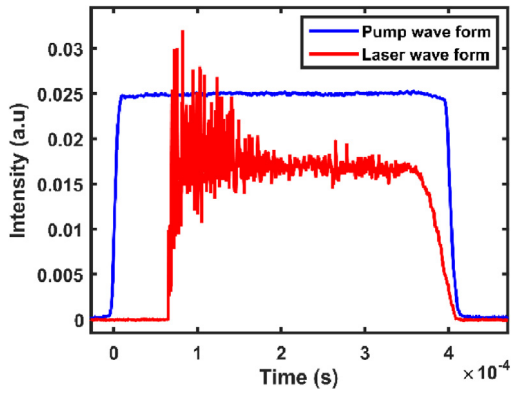

Fig. 3. The wave forms of pump and laser pulse with duty factor 7% and the width of pump pulse 398 μs.

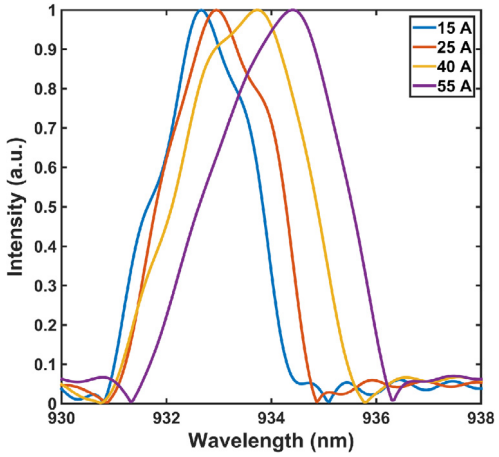

Fig. 4. Measured laser spectrum of diode laser at the temperature of 20 °C, pulse width of 230 μs, repetition rate of 20 Hz.

3. Numerical solution

The rate equations including the reabsorption of the terminated laser state in steady state can be described as [15,16]:

$$\frac{\partial N_{\mathrm{up}}}{\partial t} = \left[\sigma_{\mathrm{ab}}\left(\lambda_{\mathrm{P}}\right) N_{\mathrm{Low}} - \sigma_{\mathrm{em}}\left(\lambda_{\mathrm{P}}\right) N_{\mathrm{up}}\right] \frac{I_{\mathrm{P}}}{h\nu_{\mathrm{p}}} + \left[\sigma_{\mathrm{ab}}\left(\lambda_{\mathrm{L}}\right) N_{\mathrm{Low}} - \sigma_{\mathrm{em}}\left(\lambda_{\mathrm{L}}\right) N_{\mathrm{up}}\right] \frac{I_{\mathrm{L}}}{h\nu_{\mathrm{L}}} - \frac{N_{\mathrm{up}}}{\tau_{\mathrm{f}}} \tag{1}$$

$$\frac{\partial I_{\mathrm{L}}}{\partial t} = \left\{ c\frac{l}{\mathrm{L}'}\left[\sigma_{\mathrm{em}}\left(\lambda_{\mathrm{L}}\right) N_{\mathrm{up}} - \sigma_{\mathrm{ab}}\left(\lambda_{\mathrm{L}}\right) N_{\mathrm{Low}}\right] - \frac{1}{\tau_{\mathrm{c}}} \right\} I_{\mathrm{L}} \tag{2}$$

where I_{P} is the pump intensity, I_{L} is the average intra-cavity laser intensity, $h\nu_{\mathrm{p}}$ and $h\nu_{\mathrm{L}}$ are the pump and the laser photon energies respectively, τ_{f} is the upper manifold lifetime, c is the speed of light, l is the laser medium length, L' is the optical length of the cavity, τ_{c} is the laser photon lifetime in the cavity. The laser output at wavelength λ_{L} is:

$$I_{\mathrm{out}}\left(\lambda_{\mathrm{L}}\right) = \frac{(1-R)\, I_{\mathrm{L}}\left(\lambda_{\mathrm{L}}\right)}{2} \tag{3}$$

where R is the reflectivity of the output coupler.

The energy emitted by the laser at wavelength λ_{L} during the pump width is:

$$E_{\mathrm{out}}\left(\lambda_{\mathrm{L}}\right) = \int_0^{t_w} I_{\mathrm{out}}\left(\lambda_{\mathrm{L}}\right) Sc\, d\mathrm{t} \tag{4}$$

where Sc is the area of the output laser beam.

The temperature distribution inside the gain medium follow the heat conduction equation:

$$\rho C\frac{\partial T}{\partial t} - \nabla\cdot(K\nabla T) = Q(x,y,z,t) \tag{5}$$

where T is the temperature of laser crystal, K is the thermal conductivity of the gain medium, ρ is the mass density, C is the specific heat, Q is the heat source density.

The thermal source density with top-hat distribution can be expressed as the following:

$$Q(r,z) = \begin{cases} \dfrac{\xi P_{\mathrm{in}}}{\pi w_{\mathrm{P}}^2}\sigma_{\mathrm{ab}} N_{\mathrm{t}} \exp\left(-\sigma_{\mathrm{ab}} N_{\mathrm{t}} z\right), & r < R_{\mathrm{P}} \\ 0, & R_{\mathrm{P}} < r < R \end{cases} \tag{6}$$

where ξ is fractional thermal load, P_{in} is incident pump power, w_{P} is the radius of pump beam, σ_{ab} is the absorption cross section at pump wavelength λ_{P}, N_{t} is the total doping concentration of Yb^{3+} in laser crystal. For the convenience of solving equations, the distribution of pump beam is presumed homogeneous. R_{P} is a radius of pump spot, R is a radius of the thin disk crystal.

For the end-pumped microchip lasers system cooled by heat sink at a single side, we assume that another side surface of the disk is heat-insulated. The boundary conditions are:

$$K\nabla T = h\left(T - T_0\right) \tag{7}$$

where h is the heat exchange coefficient of disk crystal with cooling liquid. T_0 is the temperature of coolant.

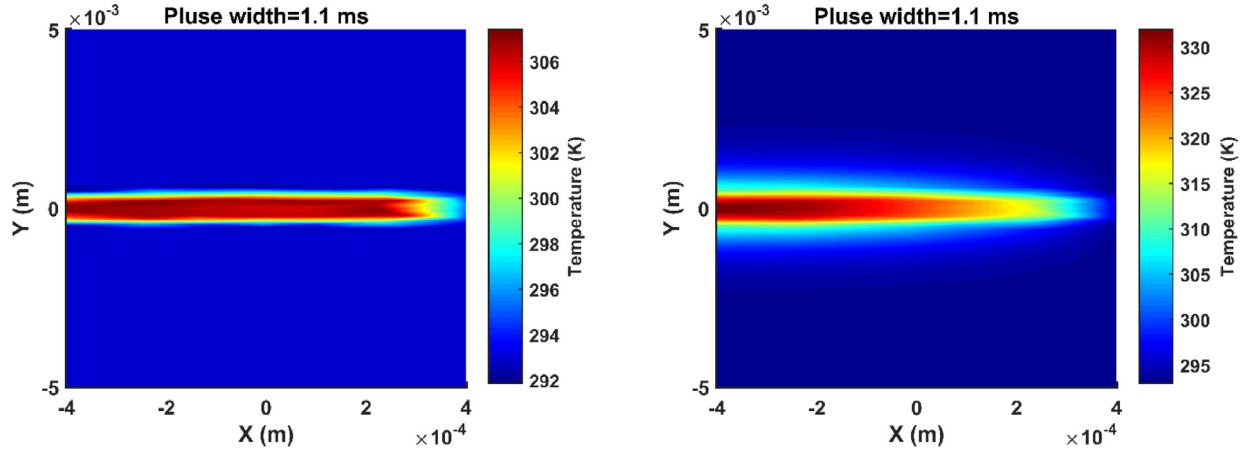

Fig. 5. Temperature profile distribution along the thickness and radius of Yb:YAG crystals under 40 A current pumping at the end of the time of pump pulse (left: first pulse, right: balance state).

Transient temperature of Yb:YAG crystal was numerically calculated. Because there are several layers of different materials between the Yb: YAG crystal and heat sink, it was difficult to obtain the accurate heat transfer coefficients. Material layers between the Yb: YAG crystal and heat sink also have been ignored. The distribution of the heat generation along longitudinal direction have been considered to be non-uniform because the absorption of crystal to the pump light followed Lambert–beer's law. Furthermore, the absorption cross-section of crystal changes with the temperature. The absorption cross-section was calculated in the step of each iteration. The laser material that was cut along longitudinal direction and was treated as a 2D rectangle under this simulation. The rectangle was divided into grids along pump direction by finite element analysis(FEA) method.

The temperature-dependency of absorption cross-section and stimulated emission cross section of Yb:YAG crystal was reported by J. Koerner and coauthors [17]. Accurate values of the emission and absorption cross sections of Yb:YAG as a function of temperature between room temperature and 200 °C are presented by a setup optimized to reduce the effect of radiation trapping.

The functional form of the fit was investigated. The temperature-dependency of absorption cross-section in pump wavelength of the crystal is given by the following formulae [18]:

$$\sigma_{\mathrm{ab}}(T)=\left[2.07+6.37\exp\left(-\frac{T-273}{288}\right)\right]10^{-21}\ \mathrm{cm}^2 \tag{8}$$

The relationship between the stimulated emission cross section of Yb:YAG crystal and temperature can be described as [19]:

$$\sigma_{\mathrm{em}}(T)=\left[2+\frac{10.5}{1+\exp\left(-\frac{\mathrm{T}-131.6}{52}\right)}\right]10^{-20}\ \mathrm{cm}^2 \tag{9}$$

Thermalization process of the levels is presumed very rapid, and the relative populations of the levels in both the upper and the lower manifolds can be described by a Boltzmann distribution. The Boltzmann distribution factor of the terminated laser level is:

$$f_{z3}=\frac{\exp\left(-\frac{E_{z3}}{kT}\right)}{\sum_{i=1}^{4}\exp\left(-\frac{E_{zi}}{kT}\right)} \tag{10}$$

where k is the Boltzmann constant, T is the temperature, E_{zi} is the energy for each Stark level of ground manifold, $i=1,\ldots,4$.

With laser working, crystal temperature will be changed. At time t, Boltzmann distribution factor is:

$$f_{z3}(t)=\frac{\exp\left(-\frac{E_{z3}}{kT(t)}\right)}{\sum_{i=1}^{4}\exp\left(-\frac{E_{zi}}{kT(t)}\right)} \tag{11}$$

Table 1
Numerical values of the parameters.

Pump wavelength	940 nm
Output wavelength	1030 nm
Laser medium thickness	0.8 mm
Yb^{3+} concentration	6.9×10^{20} cm^{-3}
Output mirror reflectivity	0.95
Upper manifold lifetime of Yb:YAG	0.95 ms [20]
Pump absorption cross section	0.76×10^{-20} cm^2 [16]
Pump emission cross section	0.22×10^{-20} cm^2 [16]
Absorption cross section at 1030 nm	0.167×10^{-20} cm^2 [16]
Emission cross section at 1030 nm	2.5×10^{-20} cm^2 [16]
Fractional thermal load	14.6% [21]
Thermal conductivity of Yb:YAG	0.014 W/(mm K) [22]
Heat exchange coefficient of back surface	1×10^{6} W/(m^2 K)

When t = 0, Boltzmann distribution factor is:

$$f_{z3}(t_0)=\frac{\exp\left(-\frac{E_{z3}}{kT(t_0)}\right)}{\sum_{i=1}^{4}\exp\left(-\frac{E_{zi}}{kT(t_0)}\right)} \tag{12}$$

When t = t_1, Boltzmann distribution factor is:

$$f_{z3}(t_1)=\frac{\exp\left(-\frac{E_{z3}}{kT(t_1)}\right)}{\sum_{i=1}^{4}\exp\left(-\frac{E_{zi}}{kT(t_1)}\right)} \tag{13}$$

The factor β is introduced, which is the ratio of Boltzmann distribution factor f_{z3} at $t=0$ and t = t_1:

$$\beta=\frac{f_{z3}(T(t_1))}{f_{z3}(T(t_0))} \tag{14}$$

Thus, the rate equations including the reabsorption of the ground state and temperature-dependent thermal population distribution can be described as:

$$\frac{\partial N_{\mathrm{up}}}{\partial t}=\left[\sigma_{\mathrm{ab}}(\lambda_{\mathrm{P}},T)N_{\mathrm{Low}}-\sigma_{\mathrm{em}}(\lambda_{\mathrm{P}})N_{\mathrm{up}}\right]\frac{I_{\mathrm{P}}}{h\nu_{\mathrm{p}}} +\left[\sigma_{\mathrm{ab}}(\lambda_{\mathrm{L}})\beta N_{\mathrm{Low}}-\sigma_{\mathrm{em}}(\lambda_{\mathrm{L}},T)N_{\mathrm{up}}\right]\frac{I_{\mathrm{L}}}{h\nu_{\mathrm{L}}}-\frac{N_{\mathrm{up}}}{\tau_{\mathrm{f}}} \tag{15}$$

$$\frac{\partial I_{\mathrm{L}}}{\partial \mathrm{t}}=\left\{c\frac{l}{L'}\left[\sigma_{\mathrm{em}}(\lambda_{\mathrm{L}},T)N_{\mathrm{up}}-\sigma_{\mathrm{ab}}(\lambda_{\mathrm{L}})\beta N_{\mathrm{Low}}\right]-\frac{1}{\tau_{\mathrm{c}}}\right\}I_{\mathrm{L}} \tag{16}$$

The values of computation parameters above were listed in Table 1.

4. Results and discussions

Temperature profile distributions along the thickness and radius of Yb:YAG crystals under 40 A current pumping were shown in Fig. 5,

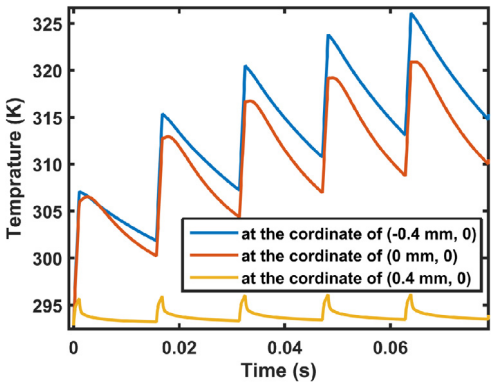

Fig. 6. Transient temperature as a function of time with different longitudinal positions at pump width of 1.1 ms. The cooling surface was located at the axis of 0.4 mm.

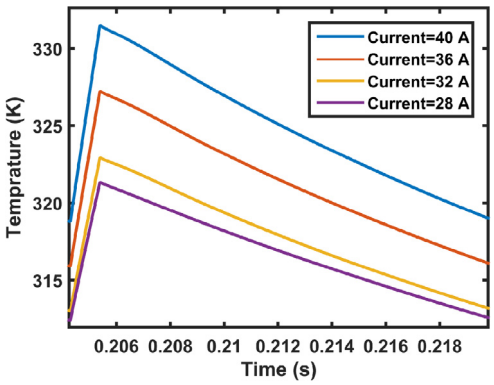

Fig. 8. Transient temperature of the front surface of laser crystal under the conditions of different pump current.

when time at the left picture was at the end of the first pump pulse and time at the right picture was at the end of the pump pulse with thermal balance state. In comparison with the right picture in Fig. 5, the left picture presented a more homogeneous temperature profiles. Because the pump light passes through the Yb:YAG crystal twice, due to 940 nm HR-coating at the back surface and the heat should be difficult to be removed during a few of pump pulse. The maximum temperature rise located at the entrance and decreased with closing to the cooled surface. The inhomogeneous temperature was caused by the method of asymmetric cooling.

Fig. 6 presented the evolution of transient temperatures of laser crystal at the different longitudinal position under the conditions of pump width of 1.1 ms, and duty cycle of 7% for the duration of first five pulses. Fig. 6 indicated that the temperature of crystal layer close to the back surface reached the balanced stage faster than that close to the front surface. With the number of pump pulse augmenting, more heat was accumulated in the position further away from the cold side, the thermal dispersion became worse.

The transient temperature simulation results were shown in Figs. 7 and 8 under lasing condition. Fig. 7 displayed transient temperatures of laser crystals at the center of front side for the same duty cycle of 7% and different pump width of 1.1 ms, 622 μs, 398 μs, 291 μs and 184 μs. The pump current was set to 40 A. The figure on the right hand side shows the temperature evolution at the same position by different pulsewidth, when the system reached the thermal equilibrium. Fig. 7 indicated that the crystal realized the thermal balance state after 0.2 s under the condition describing on above. The maximum difference of temperature between the crystal and the coolant was about 40 K. These results are consistent with literature reported by [23]. The amplitude of the fluctuation of temperature was significantly larger at long pump pulse width than that at short pump pulse width. Fig. 8 showed transient temperatures of the front surface layer of the laser crystals with different pump current under one pump period in duty cycle 7%.

The rise of crystal temperature was fast in the beginning and gradually reached a stable state where the temperature iterates up and down in the same repetition rate with pump laser. All heat of Yb:YAG crystal was removed before next pump pulse in rate equations. This process corresponds to the thermal equilibrium in Figs. 7 and 8. Obviously, Yb:YAG crystal should attain to this stage at QCW mode.

In this work, we mainly studied the output power, the threshold of pump intensity of this microchip laser and the temperature of crystal under the condition of a low duty cycle of 7% and a high duty cycle of 50%. Due to a limitation of chopper wheel, the narrowest pump pulse width was 1.1 ms when duty cycle was 50%. While the longest pump pulse width for duty cycle of 7% was 1.1 ms.

Fig. 9 showed the output powers of microchip laser operating with duty cycles of 7% and 50% under conditions of different pump pulse width and the current of pump source. Comparing with different pump current in Fig. 9(a) and (b), the output power approximately increased linearly with current of pump laser; but the increments of output power deviated significantly from linear increasing with the pump pulse width. Output power with duty cycle of 7% was relatively larger slope efficiency with the pump pulse width. The laser performance could be improved by increasing the pump width while keeping duty cycle the same. The maximum optical-to-optical efficiency of 15.6% was achieved under the condition of the pump power of 10.1 W, the pump width of 1.1 ms and the duty cycle of 7%. In comparison with 7% duty cycle, the maximum optical-to-optical efficiency decreased to 9.7% at 50% duty

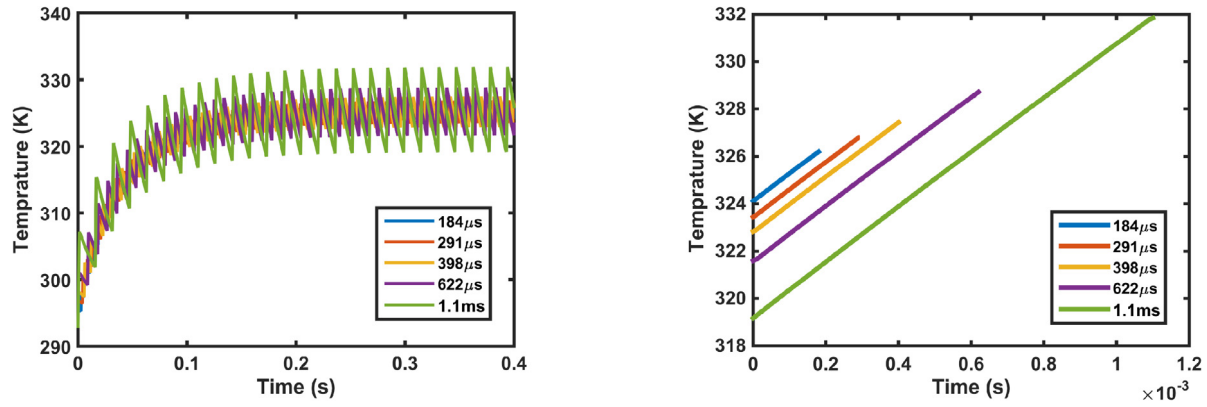

Fig. 7. Transient temperatures of laser crystals at the center of front side for the same duty cycle of 7% and different pump width of 1.1 ms, 622 μs, 398 μs, 291 μs and 184 μs. The Figure on the right was the temperatures at the same position, when the system reached the thermal balance state.

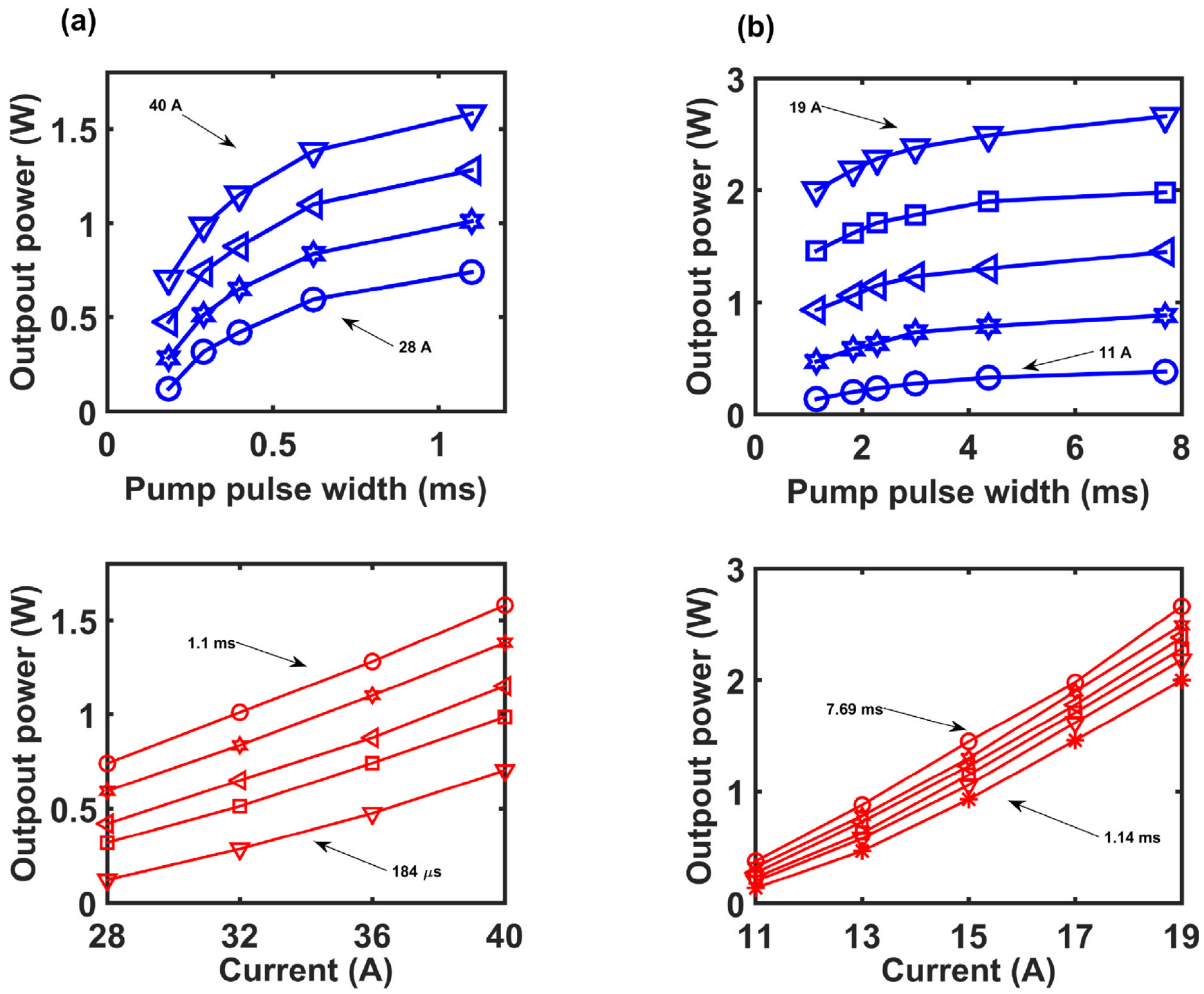

Fig. 9. Output power of Yb:YAG microchip lasers as a function of the pump pulse width and current of pump diode laser at duty cycle of 7% and 50%.

cycle. Because the heat load was rising with the increment of the duty cycle and more heat load reduced population inversion density.

The calculated and experimental pump power thresholds for output of 1030 nm were shown in Fig. 10. The filled red circles were experimental data points, while the blue solid line was from the calculation. The threshold signals of laser were detected by PD2 in experiment. The pump power threshold at long pump width was lower than that at the short pump width. The theoretical results were broadly consistent with the experimental data. In comparison with short width of the pump pulse, the long width had a relatively large discrepancy between theoretical results and experiment, as indicated in Fig. 10. The major reason for this discrepancy was as the following: the output of laser signal must be above the detecting threshold of PD2; while the total gain needed to be only slightly higher than the total loss for the theoretical pump threshold. The possible reason was the increasing thermal population of laser terminal level due to ascending transient temperature within the pump time.

The output powers of Yb:YAG lasers as a function of pump widths at different currents of pump source by theoretical calculation and experiment were shown in Fig. 11, Fig. 11 also presented simulation results of rate equations with or without the consideration of the temperature terms. As shown in Fig. 11, when the temperature term was considered, the output power has declined. The theoretical results with temperature terms were in good agreement with the experimental data, when the intra-cavity loss was about 3%. The difference between the experiment and theory was slightly bigger at current 28 A than that at current 40 A. This may be caused by the variation of mode volume and the red shift of center wavelength of the pump light with increment of

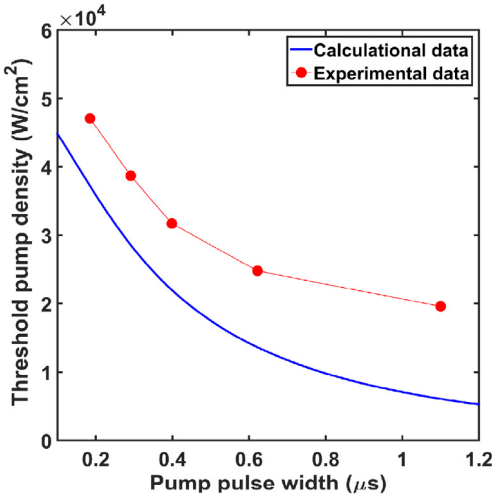

Fig. 10. Threshold pump density of Yb:YAG microchip lasers as a function of the pump pulse width at 7% duty cycle.

pump current. The laser beam was presented at Fig. 2 and could be used for calculating the area of laser in cavity. The area of laser was equal to the pump laser approximately. However, the mode volume of laser will be decreased, when the pump current was tended to the laser threshold. The center wavelength of the diode laser moved towards to 940 nm,

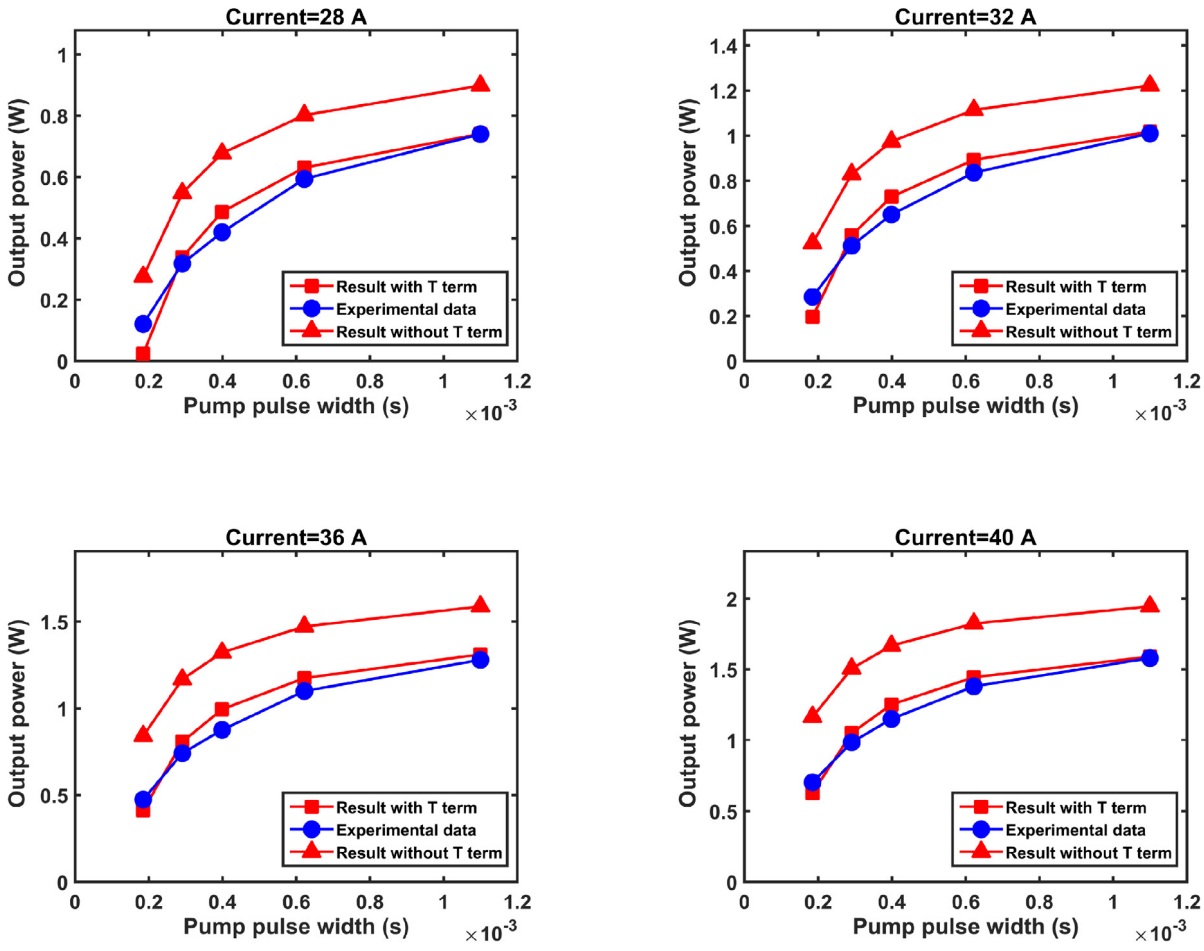

Fig. 11. Comparison of experimental results and the numerical simulations of the output power of Yb:YAG microchip lasers under different pump currents and pulse widths.

when the pump current reached 55 A as shown in Fig. 4. Although one of the advantages of Yb:YAG was broad absorption spectrum, the center wavelength of pump light did not locate at the center of the absorbed spectrum of Yb:YAG under our experimental condition.

5. Conclusion

In conclusion, the transient temperature distribution was simulated. In this simulation, the non-uniform absorption of pump light based on Lambert–beer's law and the temperature-dependency of absorption cross-section were taken into account. The effects of transient temperature of gain medium for quasi-three level microchip lasers were investigated. The numerical results reveal not only the dynamics characteristic of lasing levels, but also the relation between pump pluses width and output power. The effect of transient temperature of laser materials on output power was discussed. Because the heat load was rising with the increase of the duty cycle and high heat load reduced population inversion density, the optical-to-optical efficiency of 9.7% at 50% duty cycle was lower than optical-to-optical efficiency of 15.6% at 7% duty cycle. As the result, the output power calculated by the model with the consideration of heat terms was lower than that by the model without heat terms. The calculated and experimental pump power thresholds for output of 1030 nm was discussed. The theoretical results were broadly consistent with the experimental data. A comparison between the calculated results and experiments reveals that this model in equivalent duty cycle was quite coincident for the experimental results of Yb:YAG microchip laser.

However, our theoretical model was based on one-dimension rate equations for quasi-three level systems. This model did not take into account the distribution of pump light and output laser, the temperature distribution and temperature-dependent thermal conductivity. The calculated results were in accord with experiments and certify that this model was more practical to quasi-three level QCW systems with pulse pumping.

Acknowledgment

This work was supported by the National Natural Science Foundation of China (Grant Nos. 11304311, 11475177, 61505210).

References

[1] J. Dong, A. Shirakawa, K.I. Ueda, A.A. Kaminskii, effect of ytterbium concentration on cw ybyag microchip laser performance at ambient temperature, Appl. Phys. B 89 (2007) 359–365.
[2] W. Koechner, Solid-State Laser Engineering, Springer-Verlag, Berlin, 2006.
[3] R. Platz, B. Eppich, J. Rieprich, W. Pittroff, G. Erbert, P. Crump, High duty cycle, highly efficient fiber coupled 940-nm pump module for high-energy solid-state lasers, High Power Laser Sci. Eng. 4 (2016) 5.
[4] L. Esposito, J. Hostasa, A. Piancastelli, G. Toci, D. Alderighi, M. Vannini, T. Epicier, A. Malchere, G. Alombert-Goget, G. Boulon, Multilayered YAG-Yb:YAG ceramics: manufacture and laser performance, J. Mater. Chem. C 2 (2014) 10138–10148.
[5] T.Y. Fan, Heat-generation in Nd-YAG and Yb-YAG, IEEE J. Quantum Electron. 29 (1993) 1457–1459.
[6] M. Innocenzi, H. Yura, C. Fincher, R. Fields, Thermal modeling of continuous-wave end-pumped solid-state lasers, Appl. Phys. Lett. 56 (1990) 1831–1833.
[7] A.K. Cousins, Temperature and thermal-stress scaling in finite-length end-pumped laser rods, IEEE J. Quantum Electron. 28 (1992) 1057–1069.
[8] M. Schmid, T. Graf, H.P. Weber, Analytical model of the temperature distribution and the thermally induced birefringence in laser rods with cylindrically symmetric heating, J. Opt. Soc. Am. B-Opt. Phys. 17 (2000) 1398–1404.

[9] S.Z. Shuja, B.S. Yilbas, S.Z. Shazli, Laser repetitive pulse heating influence of pulse duty on temperature rise, Heat Mass Transf. 43 (2007) 949–955.
[10] J.L. Li, J. Dong, M. Mitsurua, A. Shirakawa, K. Ueda, Transient temperature profile in the gain medium of CW- and end-pumped passively Q-switched microchip laser, Opt. Commun. 270 (2007) 63–67.
[11] S.Z. Shuja, B.S. Yilbas, Laser heating of a moving slab: Influence pulse intensity parameter on temperature and stress fields, Opt. Laser Technol. 70 (2015) 7–16.
[12] G.Z. Zhu, X. Zhu, Y. Huang, H.L. Wang, C.H. Zhu, Numerical analysis of an end-pumped Yb:YAG thin disk laser with variation of a fractional thermal load, Appl. Opt. 53 (2014) 4349–4358.
[13] X.J. Cheng, J.L. Wang, B.X. Jiang, Thermal analysis on grad-doped active-mirror Yb:YAG ceramic lasers, Opt. Eng. 54 (2015) 3.
[14] P. Ferrara, M. Ciofini, L. Esposito, J. Hostasa, L. Labate, A. Lapucci, A. Pirri, G. Toci, M. Vannini, L.A. Gizzi, 3-D numerical simulation of Yb:YAG active slabs with longitudinal doping gradient for thermal load effects assessment, Opt. Express 22 (2014) 5375–5386.
[15] O. Casagrande, N. Deguil-Robin, B. Le Garrec, G.L. Bourdet, Time and spectrum resolved model for quasi-three-level gain-switched lasers, IEEE J. Quantum Electron. 43 (2007) 206–212.
[16] T. Fan, R. Byer, Modeling and CW operation of a quasi-three-level 946 nm Nd: YAG laser, IEEE J. Quantum Electron. 23 (1987) 605–612.
[17] J. Koerner, C. Vorholt, H. Liebetrau, M. Kahle, D. Kloepfel, R. Seifert, J. Hein, M.C. Kaluza, Measurement of temperature-dependent absorption and emission spectra of Yb:YAG, Yb:LuAG, and Yb:CaF2 between 20 degrees C and 200 degrees C and predictions on their influence on laser performance, J. Opt. Soc. Am. B-Opt. Phys. 29 (2012) 2493–2502.
[18] Q. Liu, X. Fu, M. Gong, L. Huang, Effects of the temperature dependence of absorption coefficients in edge-pumped Yb : YAG slab lasers, J. Opt. Soc. Am. B-Opt. Phys. 24 (2007) 2081–2089.
[19] J. Dong, M. Bass, Y.L. Mao, P.Z. Deng, F.X. Gan, Dependence of the Yb3+ emission cross section and lifetime on temperature and concentration in yttrium aluminum garnet, J. Opt. Soc. Am. B-Opt. Phys. 20 (2003) 1975–1979.
[20] D.S. Sumida, T.Y. Fan, Effect of radiation trapping on fluorescence lifetime and emission cross-section measurements in solid-state laser media, Opt. Lett. 19 (1994) 1343–1345.
[21] M.J. Dashcasan, E. Barati, Power scaling limitations in quasi-three level thin gain lasers, Opt. Laser Technol. 45 (2013) 480–487.
[22] J. Rafiei, J. Sabbaghzadeh, I.M. Asl, S.S. Kazemi, Three-dimensional modeling of thermo-mechanical finite element analysis in edge-pumped composite Yb:YAG/YAG thin-disk laser, Opt. Commun. 283 (2010) 3469–3474.
[23] X.H. Lu, J.F. Wang, Y.E. Jiang, W. Fan, X.C. Li, Transient thermal effects in end-pumped cryogenic Yb:YAG regenerative amplifier, J. Modern Opt. 59 (2012) 354–359.